Flow-Induced Transport via Optical Heating of a Single Gold Nanoparticle

Jun-ichi Chikazawa,[†] Takayuki Uwada,[‡] Akihiro Furube,[†] and Shuichi Hashimoto*[,†]

[†] Department of Optical Science, University of Tokushima, 2-1 Minami-Josanjima-cho, Tokushima 770-8506, Japan.

[‡] Department of Chemistry, Josai University, 1-1 Keyakidai, Sakado, Saitama 350-0295, Japan.

Abstract

Optothermal trapping has gained increasing popularity in manipulation such as selecting, guiding, and positioning submicron objects because of a few mW laser power much lower than that required for optical trapping. The optotothermal trapping uses thermal gradient-induced phoretic motions, but the underlying physics of driving force has not been fully understood. In this study, we performed optotothermal trapping of 500-nm-diameter colloidal silica via a continuous laser illumination of a single gold nanoparticle from the bottom in a closed chamber. Under illumination, the tracer particles were attracted to the gold nanoparticle and trapped. Notably, the direction of migrating particles was always to hot gold nanoparticle regardless of the configuration of gold nanoparticle placed at two opposite sides of the chamber, on the bottom surface of an upper substrate (ceiling) or on the top surface of a lower substrate (floor). The previous interpretation based on thermal convective flow from the bottom to the top and circulating inside the chamber was only applicable to floor configuration and failed to explain our observation for ceiling. Instead, temperature-induced Marangoni effect at the water/superheated water interface is likely to play a role. This study promoted a better understanding of the driving mechanism in optothermal trapping. Moreover, as an application of the single-particle platform, we showed the photothermal phase separation-induced microdroplet formation of thermoresponsive polymers and the coating of non-thermoresponsive polymers on nanoparticles.

Introduction

Plasmonic nanoparticles (NPs) have emerged as unique nanoheaters that selectively heat the local environment of the particles.[1,2] This local heating finds various applications - from photothermal cancer therapy and photothermal imaging to photothermally-enhanced catalytic activity and photothermal thermoelectric devices.[3-6] Continuous laser heating of a plasmonic NP results in a well-defined steady-state temperature profile, $\Delta T \propto r^{-1}$, in the surrounding environment,[7] but above all, thermal field thus generated exhibits a non-equilibrium nature: heat generation at the heating center with simultaneous heat dissipation through heat transfer towards the outside regions. This non-equilibrium thermal field with extremely large temperature gradient can induce a microfluidic flow and a phoretic motion, potentially offering dynamic environment for small-scale physical and chemical processes such as mixing, phase separation and crystallization.[1]

Thanks to a fluidic and phoretic flow generated by the temperature gradient, optothermal trapping[8] has been used as a manipulation technique such as selecting, directing, and positioning micron-size objects and NPs because of a fascinating low ~mW input-power alternative to high 10^2 – 10^3 mW used in laser trapping relying upon an optical gradient force.[9-11] As a driving mechanism of molecular migration under the temperature gradient, thermal convection,[12] thermophoresis,[8] and thermocapillary or Marangoni effect[13] has been widely accepted but these forces may work in a complex manner, making it difficult to pinpoint underlying physics.[14]

Previously, when a single gold nanoparticle (Au NP) supported on a transparent substrate and submerged in aqueous solutions of polyethylene glycol (MW: 6000; PEG 6000) and sodium dodecyl sulfate (SDS) were exposed to laser illumination causing the NP heating, migration and accumulation of solutes, PEG 6000 and SDS, were observed, forming a Au NP core-organic shell particle.[15] Moreover, thermoresponsive polymers represented by poly(*N*-isopropylacrylamide) (PNIPAM) and poly(vinylmethylether) (PVME) have exhibited a reversible microdroplet formation surrounding a Au NP for heating/cooling due to on/off laser light.[16,17] For the PNIPAM microdroplet, at least 50 times greater concentration than that of bulk solution was attained. The observed particle

heating-induced reversible/irreversible accumulation of solutes suggested the occurrence of thermal gradient-driven forces or liquid flows, leading to molecular transport toward a hot Au NP. The technique may open a potential to fabricate various coated NPs or to induce microscale phase separation. However, the driving mechanism has been only poorly understood, and the fundamental question that why molecules were attracted to a hot spot, resulting in accumulation, still remains unsolved. We assume that the observed accumulation is caused by optothermal trapping that attracts the molecules to the hot area, thus further experimental proof is necessary.

In this study, we used an aqueous submicron colloidal suspension to visualize the driving forces or liquid flows around a hot Au NP through tracking of individual particles. For simplicity, we used no additives that may reverse the migration direction of colloids through depletion interaction[18,19] or thermoelectricity.[20,21] Thermophoresis is a motion of particles subjected to temperature gradient. Without additives in aqueous solution, the direction of thermophoresis is from hot to cold for a great majority of macromolecules and colloids at temperatures > 4°C because the thermophoresis is driven by the thermal expansion of water.[22,23] This results in positive Soret coefficient, $S_T > 0$ because of positive D_T ($S_T = D_T/D$ where S_T represents the thermophoretic mobility, D_T, the thermal diffusion coefficient, and D, the Brownian diffusion coefficient). Negative S_T or D_T is defined as the movement from cold to hot. For interpreting the experimental observation of migration to a hot Au NP using the thermophoresis, a negative S_T should be assumed for cases where a positive S_T has been measured for PEG,[24] SDS[25] and PNIPAM,[26] which is contradictory.

By contrast, thermal convection- and Marangoni convection-based interpretation appears intriguing to justify the migration directed to a hot spot.[12,13] As shown in Scheme 1, both thermal convection (a) and Marangoni convection (b) can collect particles and molecules to the heated area. Experimentally, Flores-Flores and coworkers observed that the 2D trapping of multiple silica microparticles (d=2.5 μm) in a closed chamber (100 μm gap) occurred when illuminated from the top both at low (0.8 mW) and high intensities (<11 mW where a vaper bubble was formed) through laser heating a thin film of amorphous silicon (a-Si:H) deposited on the top of a lower substrate.[12]

For interpretation, they used the thermal convection similar to Scheme 1a for low laser power trapping events whereas they assumed that Marangoni convection at air-water interface (Scheme 1b) is responsible for trapping at high laser powers where bubble formation occurred.[27-29] A similar experimental result of trapping of 500-nm-diameter polystyrene (PS) particles has been reported by Kang and coworker using a deposited Au nano-island film for heating by illuminating from the bottom.[14] However, their interpretation was based on the combined effect of thermal convection, optical gradient force, and thermophoresis.

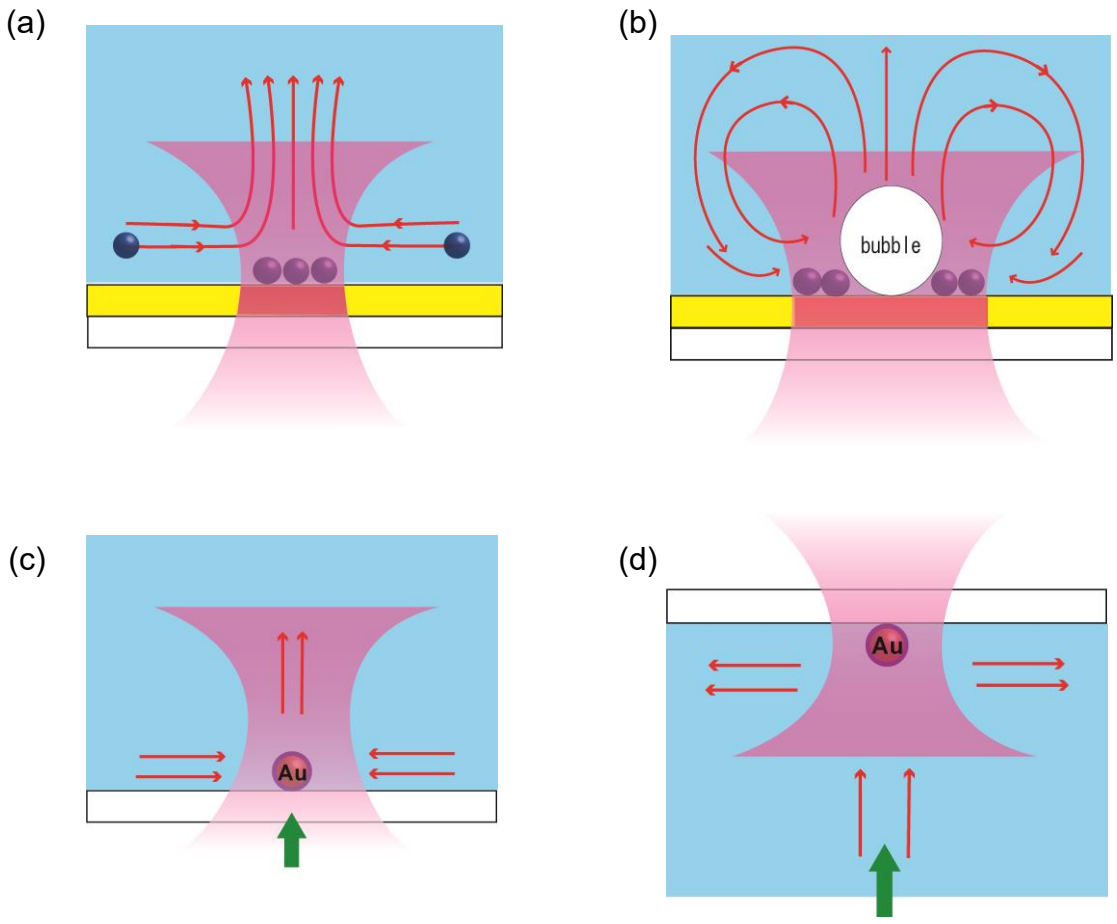

Scheme 1. (a, b) Previously proposed working physics of optothermal trapping of colloids[12]: (a) thermal convection-induced trapping and (b) bubble-induced Marangoni convection-based trapping on heating of a metallic film deposited on the bottom surface. (c, d) Hypothetical convection when a single spherical Au NP was optically heated in two configurations, floor (c) and ceiling (d). Red arrows represent the direction of convection and green arrows point to the illuminating laser beam.

Single NP heating has a merit of providing an ideal point heat source with a distinct radial temperature profile because of a well-defined absorption cross-section based upon the localized surface plasmon resonance (LSPR).[1] Another merit is that, besides imaging optical spectroscopic investigations can be made, which is useful for obtaining information beyond the diffraction limit of imaging optics.[16] When a single Au NP supported in two configurations, a top surface of a lower substrate (Scheme 1c, floor) and a bottom surface of an upper substrate (Scheme 1d, ceiling) in a closed chamber was illuminated, the direction of thermal convection should be revered. This will affect the motion of molecules and colloids to/from Au NP and we may gain insight into the driving mechanism. In what follows, we will describe our findings that can complement the current understanding of optothermal manipulation that may have a great potential to fabricate nanomaterials of new attribute.

Experimental Methods

Optical measurement. We used a darkfield imaging on an inverted microscope, IX71 (Olympus, Tokyo, Japan; with a darkfield condenser NA = 0.8–0.92) equipped with a DN3V-300 CMOS camera (SHODEN-SHA Co., Osaka, Japan), as given in Supporting Information, Figure S1. A halogen lamp with a broad (white) spectrum was used for illumination for recording the scattering images. A HA50 IR-cut filter (Hoya Candeo Optronics, Tokyo, Japan) was used for minimizing the lamp heating. Single Au NPs adsorbed on a top surface of a lower substrate (floor) or a bottom surface of an upper substrate (ceiling) in a closed chamber were heated by illuminating a focused 488-nm CW laser, OBIS-488-LX-50 (Coherent, Santa Clara, CA) beam through a microscope objective (60×, NA = 0.70). The single particle light scattering spectra were measured as described elsewhere.[15] The spatial laser profile was determined by measuring scattering signal intensity of the 100-nm-diameter Au NP while scanning a motorized stage at 100-nm interval. The FWHM of the laser beam thus determined was 0.6 μm. The laser peak power density I_p (mW μm^{-2}) was represented by $I_p = [P(2.3546)^2]/[2\pi(FWHM)^2]$, where P is the laser power density (measured

laser power divided by beam area). All measurements were performed at 24±1°C.

Sample preparation. Spherical Au NPs (d = 102±5 nm, Supporting Information, Figure S2) prepared by a laser reshaping technique[15] were spin-coated onto a borosilicate cover glass (Matsunami, Osaka, Japan) of 24 mm × 32 mm × 0.17 mm. The Au NPs were washed twice with double-distilled water by placing 0.5 mL of water on a spin coater and spun. Au NPs were immersed in 2.0×10^8 particles mL^{-1} aqueous suspensions of silica (HIPRESICA, UBE Exsymo Co., Tokyo Japan) or polystyrene particles (LB6, Sigma-Aldrich). The silica particles (d = 500 nm ±10%, density: 1.9 g cm^{-3}, refractive index: 1.44 at 589 nm) were abbreviated as Si-OH because of unmodified surface that is assumed to be covered with silanol groups. We used Si-OH at both pH 6~7 and pH~9; no difference was observed for the particle motion. The polystyrene particles (d = 600 nm ±10%, density: 1.05 g cm^{-3}, refractive index: 1.59 at 589 nm, unmodified surface) were abbreviated as PS. The sample chamber was prepared by sandwiching a glass substrate (0.17 mm thick), a 200-μm-thick (silicone rubber) or a 10-μm-thick (d = 10 μm silica particles) spacer, and a glass substrate (0.17 mm thick). The chamber peripheral was sealed with silicone rubber adhesive. The chamber volume is estimated to be 10-μL (200-μm thickness) or 0.5-μL (10-μm thickness). The substrates were cleaned in a boiling mixture of 1:1 30% H_2O_2 - 28% ammonia mixture for 90 min, and plasma-cleaned in a YHS-R reactor (70 W, 20 kHz; Sakigake Semiconductor, Kyoto, Japan) for 60 s just before use.

Numerical simulation. A commercial finite-element mode solver, COMSOL Multiphysics Ver. 5.4b (http://www.comsol.com), was used for temperature estimation and convective flow analysis under illumination of a focused laser beam on single Au NPs at two configurations, floor and ceiling. The schematic of simulation geometry was given in Supporting Information, Figure S3. The particle heating was stimulated based upon 2-D heat conduction coupled with thermal and Marangoni convection around the particle. Au NP of 100-nm diameter was immobilized on a glass substrate and submerged in a water film. The thickness of the water film was set at experimental 10 and 200 μm. The thickness of the glass substrate was set at 100 μm and the width of the sample well

was assumed as 1000 μm. COMSOL Material Library was used for calculations using the temperature-dependent physical parameters, thermal conductivities, heat capacities, viscosities and densities of gold, liquid water, and glass. First, temperature elevation of a Au NP illuminated with a focused CW laser light at a wavelength of 488 nm was calculated using a "heat transfer module", in which the absorption cross section of Au NP was calculated via a "RF module". The initial temperature of the system was set to 293 K. Thermal convection in water film induced by heat dissipation from hot Au NP was investigated as a function of time by solving time-dependent Navier-Stokes equations under the Boussinesq approximation (https://www.comsol.jp/multiphysics/boussinesq-approximation). The convection flow provided feedback to the temperature distribution around the particle and they eventually reached the equilibrium state within 100 ms. In the presence of a water vapor bubble that may form around a Au NP, thermal Marangoni convection flow that occurs at the bubble/water interface was simulated using a COMSOL application model "Marangoni effect" in which the temperature dependence of surface tension γ at the interface was described by:[30]

$$\gamma = 235.8\times10^{-3}\left(1-\frac{T}{T_c}\right)^{1.256}\left\{1-0.625\left(1-\frac{T}{T_c}\right)\right\}\ [Nm^{-1}] \qquad (1)$$

where T is the temperature at the interface estimated by COMSOL and T_c corresponds to the critical temperature of water (374°C or 647 K). Temperature-dependent physical properties of water vapor were obtained from elsewhere[31].

Results and Discussion

Au NP heating-induced trapping of silica (Si-OH)

Continuous laser excitation of a 100-nm-diameter single gold nanoparticle (Au NP) raises the particle temperature through the absorption of both LSPR and interband transitions,[32] allowing a

steady state temperature profile for both the particle and the surroundings[6] (see Supporting Information, Figure S4 for the estimated particle temperature vs. laser intensity). In our experiment, Au NPs were supported on a glass substrate in a closed chamber filled with a suspension of 500-nm-diameter silica or PS particles. Figure 1 shows the snapshots (darkfield images) of suspended silica particles on laser illumination at 0 s, 5 s, 20 s, and laser-off (movies corresponding to Figure 1 are given in Supporting Information, movie S1 ~ movie S4). The excitation enabled the observation of silica particles being forced to migrate to the hot Au NP, resulting in trapping next to the Au NP. The laser illumination was performed from the bottom and the laser intensities were set at 2.0 (*a*), 6.0 (*b*, *d*), and 14 mW μm^{-2} (*c*). To shed light on the role of thermal convection, Au NPs were mounted on both floor (*a*-*c*) and ceiling (*d*). Before illumination (t_1 = 0 s), the particles were moving in random directions. On starting illumination, the silica particles were strongly attracted to the Au NP forming aggregates (t_1 = 5 s). The area of trapped aggregates increased remarkably with continuous illumination (t_1 = 20 s). On terminating the illumination (*t*(off)), the silica particles were released to the solution, suggesting that the observed particle trapping is a reversible phenomenon. In *b*, the observation is similar to that in *a*, but because of 3 times the greater laser intensity, the velocity of silica particles jumping into a hot Au NP is much higher resulting in a greater number of trapped particles. Further increase in laser intensity gave much increased velocities, resulting in further bigger trapped area as shown in *c*. To explore time evolution of the trapping in detail, the number of trapped silica particles was plotted as a function of laser illumination period in Figure 1*e* at various laser intensities (see Supporting Information, Figure S5 for the images of Si-OH particles used for counting the trapped particle numbers). Trapped particles are greater in number as the laser intensity is higher as observed in Figure 1*a*–*c*. Figure 1*e* shows clearly the precise picture of the trapping event that is dependent on illumination time: the number of trapped particles increased with time initially and later saturated. From Figure 1*e*, the threshold laser intensity of trapping is estimates as 0.5 mW μm^{-2}.

(*a*)

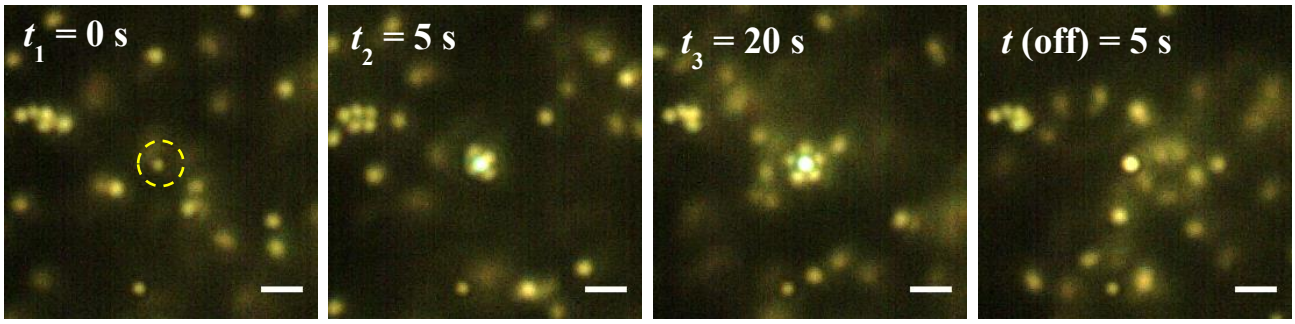
t_1 = 0 s
t_2 = 5 s
t_3 = 20 s
t (off) = 5 s

(*b*)

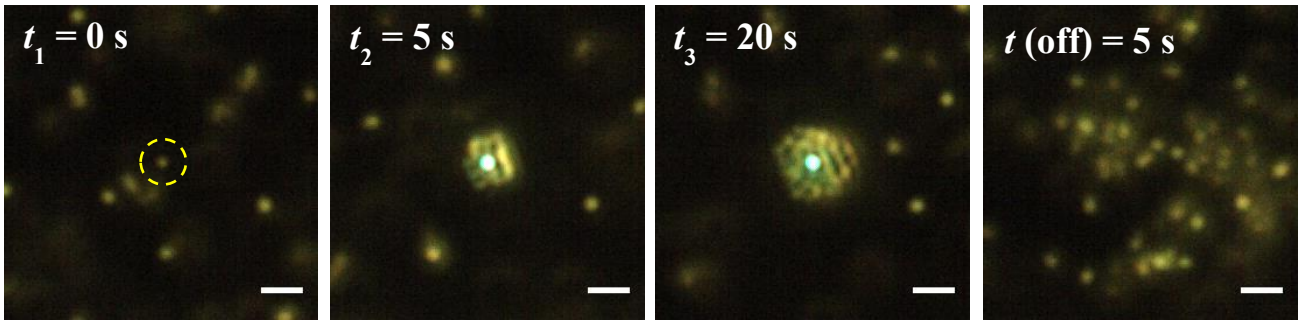
t_1 = 0 s
t_2 = 5 s
t_3 = 20 s
t (off) = 5 s

(*c*)

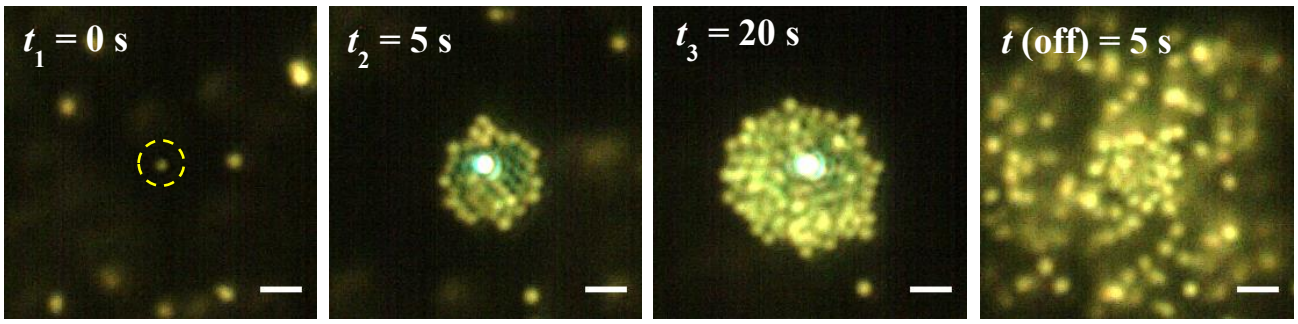
t_1 = 0 s
t_2 = 5 s
t_3 = 20 s
t (off) = 5 s

(*d*)

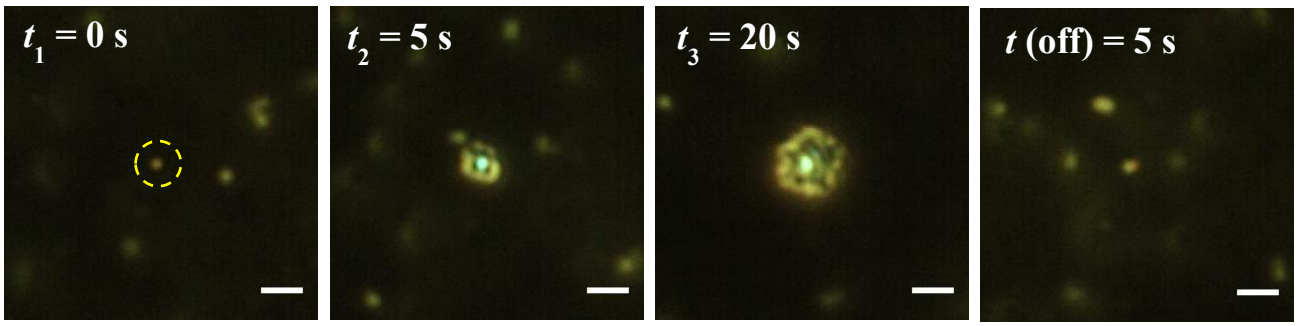
t_1 = 0 s
t_2 = 5 s
t_3 = 20 s
t (off) = 5 s

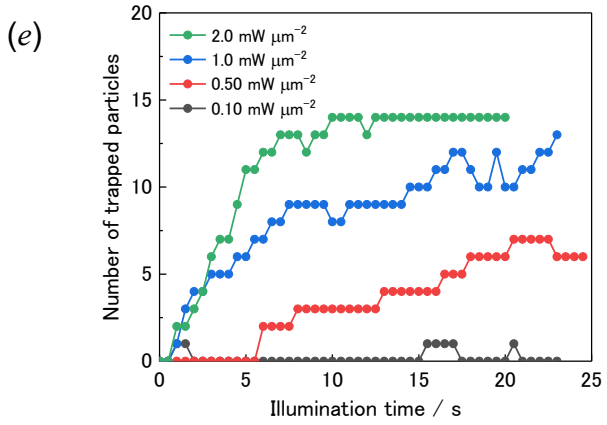

Figure 1. (*a-d*) Snapshots (darkfield microscope images) showing the trapping of 500-nm-diameter Si-OH particles on excitation of a single 100-nm-diameter Au NP supported on a glass substrate at various accumulated illumination time and after laser was blocked, and (*e*) number of trapped particles as a function of laser intensity (errors: within ±10%). Experimental parameters, water film thickness: 200 μm; laser peak power density: 2.0 mW μm^{-2} (*a*), 6.0 mW μm^{-2} (*b*, *d*), and 14 mW μm^{-2} (*c*); Au NP position in a chamber: the floor configuration (*a*, *b*, *c*), the ceiling configuration (*d*). Green spots are attenuated laser positions. Scale bars: 2 μm.

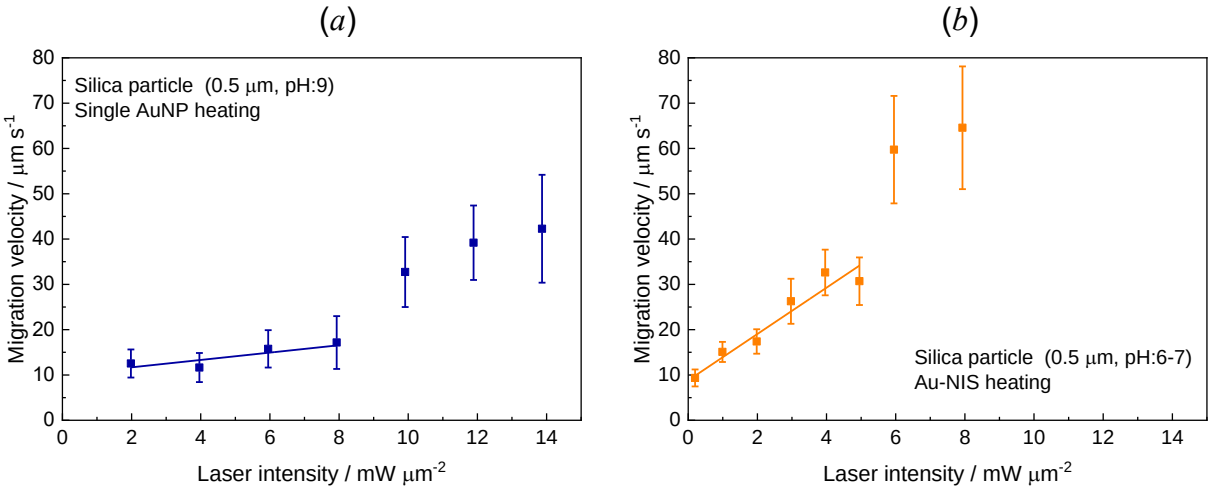

Figure 2. Migration velocity of Si-OH NP departing from 2 – 5 μm away from the heating center as a function of laser intensity; (*a*), single 100 nm Au NP; (*b*), Au nanoisland-film substrate. Solid lines are drawn as a visual guide.

To take advantage of the single particle platform, we performed the spectroscopic detection of optothermal trapping through the measurement of light scattering spectra of a Au NP. To retain an adequate level of scattering intensity during the laser illumination, we used 100-nm diameter tracer particles instead of 500-nm diameter. On laser illumination, because of an increased medium refracted index sensed by a Au NP, red-shifted scattering spectra should occur when Si-OH particles

are trapped next to the Au NP.[16] As shown in Supporting Information Figure S6, we failed to observe a red-shift compared to the spectrum of an unirradiated Au NP hampered by temperature-induced refractive index reduction in medium water.[33] Nevertheless, we observed red-shifted spectra greater than those in pure water. Although not very convincing, this can be indicative of particle trapping observed by the single particle spectroscopy.

For 500-nm PS particles, we observed that they were attracted to a hot Au NP as they approach closer to the NP with velocities lower than those observed for Si-OH particles. However, as opposed to Si-OH particles, PS particles were not stably trapped by the hot NP.

Using the particle tracking (see Supporting Information, Figure S7), we measured the velocity of each particle during the illumination. The velocity depended on the laser intensity and the radial distance from a hot Au NP. Figure 2 depicts the migration velocity in the close vicinity of a Au NP (as a guide, Si-OH particles travelling from 2 – 5 μm away from the particle) as a function of laser intensity, in comparison with the velocity of Si-OH particles observed for laser-heating a Au nanoisland film (Supporting Information, Figure S8). The velocity represents that of plunging into the hot NP. The velocity increased with an increase in laser intensity. For a single Au NP heating (Figure 2a), by far enhanced velocities were observed with significantly scattered values at laser intensities ≥ 10 mW μm^{-2}. We assume the discontinuity of the migration velocity occurred at above 10 mW μm^{-2} is indicative of photothermal bubble formation around the Au NP, despite the fact that the image of a bubble was not clearly seen in our darkfield microscopy (Figure 1c). A previous study gave a bubble generation threshold of ~10 mW μm^{-2} for the excitation of a 150-nm-diameter Au NP supported on a glass substrate and submerged in water with a illumination wavelength at 532 nm focused using an objective of NA: 0.75.[29] Such photothermal bubbles have been recognized to boost a strong Marangoni convection at the water/bubble interface,[34] resulting in the fixation of colloids and nanoparticles.[27,28,35,36] Indeed, we observed that not all but some Si-OH particles trapped during the illumination stayed there even after closing a laser shutter (Figure 1c: laser off). In contrast, the bubble formation threshold of 6.0 mW μm^{-2} thus measured for Au nanoisland film

is much smaller than that for a single Au NP (Figure 2b). This is because the heating efficiency at a given laser power is greater for the nanoisland film because of the collective heating effect.[1]

It is noteworthy that we observed the optothermal trapping of Si-OH particles for ceiling configuration, as depicted in Figure 1d (at 6.0 mW μm^{-2}). The ceiling configuration allowed the trapping of Si-OH NPs at laser intensities similar to those observed for trapping on floor configuration, including high intensities where bubble formation may occur. Thus we assume that the optothermal trapping can overcome interference from the thermal convection. This point will be discussed in detail in association with water film thickness below.

Here we focus our attention to the radial distance-dependent velocity of silica particles during laser illumination that induced optothermal trapping. Figure 3 shows the migration velocity as a function of radial distance from a hot Au NP. The laser intensity used was 6.0 mW μm^{-2} in *a* and *b*, and 2.0 or 6.0 mW μm^{-2} in *c*, below the threshold of bubble generation. Each point was rather scattered. The migration velocities towards a Au NP increased remarkably as the particles approach closer to the hot Au NP whereas the particle located away from the hot Au NP remained with low velocities in randomly oriented directions. We took a careful look at the effects of water film thickness (10 μm and 200 μm) as well as the Au NP configuration. Comparison of Figure 3*a* and 3*b* revealed that neither the film thickness nor the configuration affected the velocities of migration

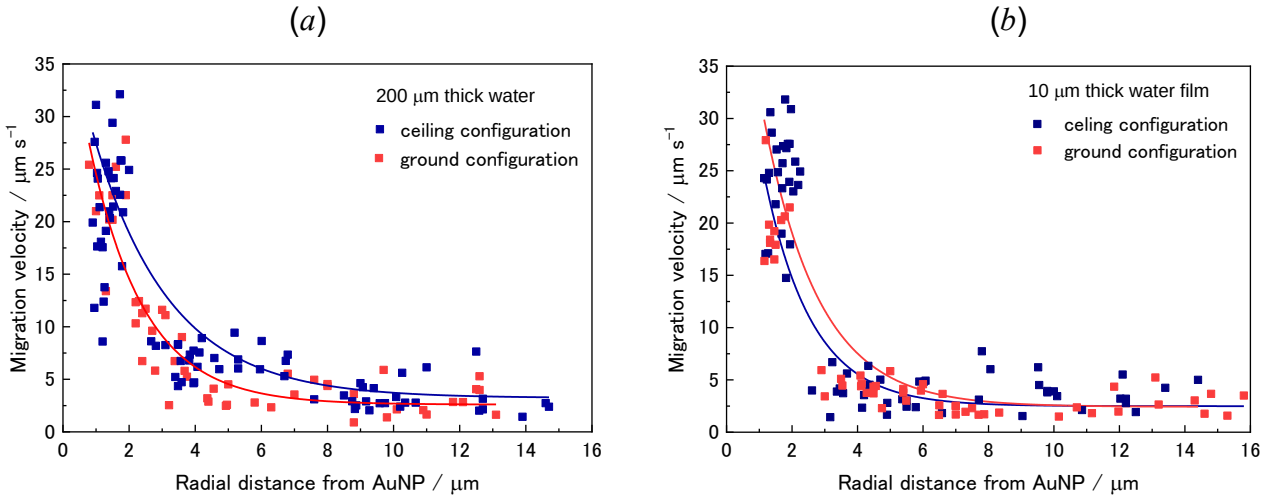

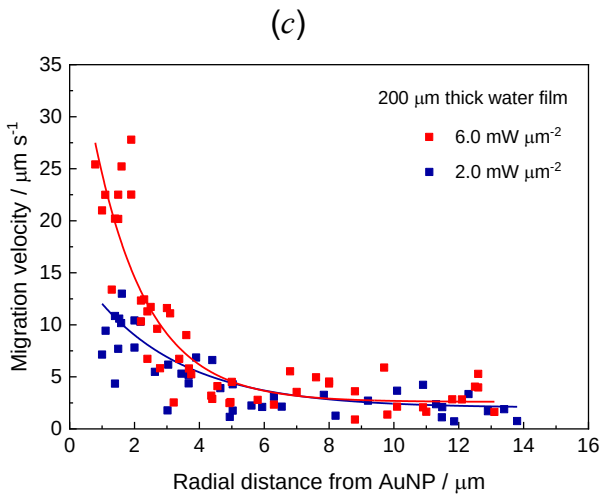

Figure 3. Effects of Au NP configuration (*a*, *b*) and laser intensity (*c*) on the migration velocity of silica particles (diameter: 500 nm, concentration: 2×10^8 particles mL^{-1}) as a function of distance from a heat source for two water film thicknesses: 200 μm (*a, c*) and 10 μm (*b*). Laser intensity: 6.0 mW μm^{-2}. (*a*, *b*) and 3.0 mW μm^{-2} (*c*). Solid lines are drawn as a visual guide. Errors in measured velocities: within ±10%.

resulting in trapping. It has been stated in the literature that such a small thickness as 10 μm resulted in a negligibly weak thermal convection.[37-39] This implies that the effect of thermal convection on the observed trapping should be minor. The conclusion is also supported by the absence of configuration effect for Au NP. If the effect of thermal convection is non-negligible, the convection directing from the lower to upper surface of the chamber followed by a flow away from a hot Au NP is in the counter direction to the migration and trapping observed at ceiling. The migration velocity in the vicinity of a Au NP is strongly affected by a laser intensity applied, as depicted in Figure 3*c*. The velocity is higher for higher laser intensity. For instance, the maximum velocity was 30 μm s^{-1} at 6.0 mW μm^{-2} whereas 15 μm s^{-1} at 2.0 mW μm^{-2}. The migration velocities at the close vicinities of Au NP were much higher when a bubble is formed around a Au NP: > 100 μm s^{-1} at maximum for 14 mW μm^{-2}.

Underlying working principle of the trapping event

Here we consider the working principle behind the optothermal trapping of Si-OH particles observed on heating a single Au NP. Figure 4*a*–*c* depicts the simulated convective flow maps under

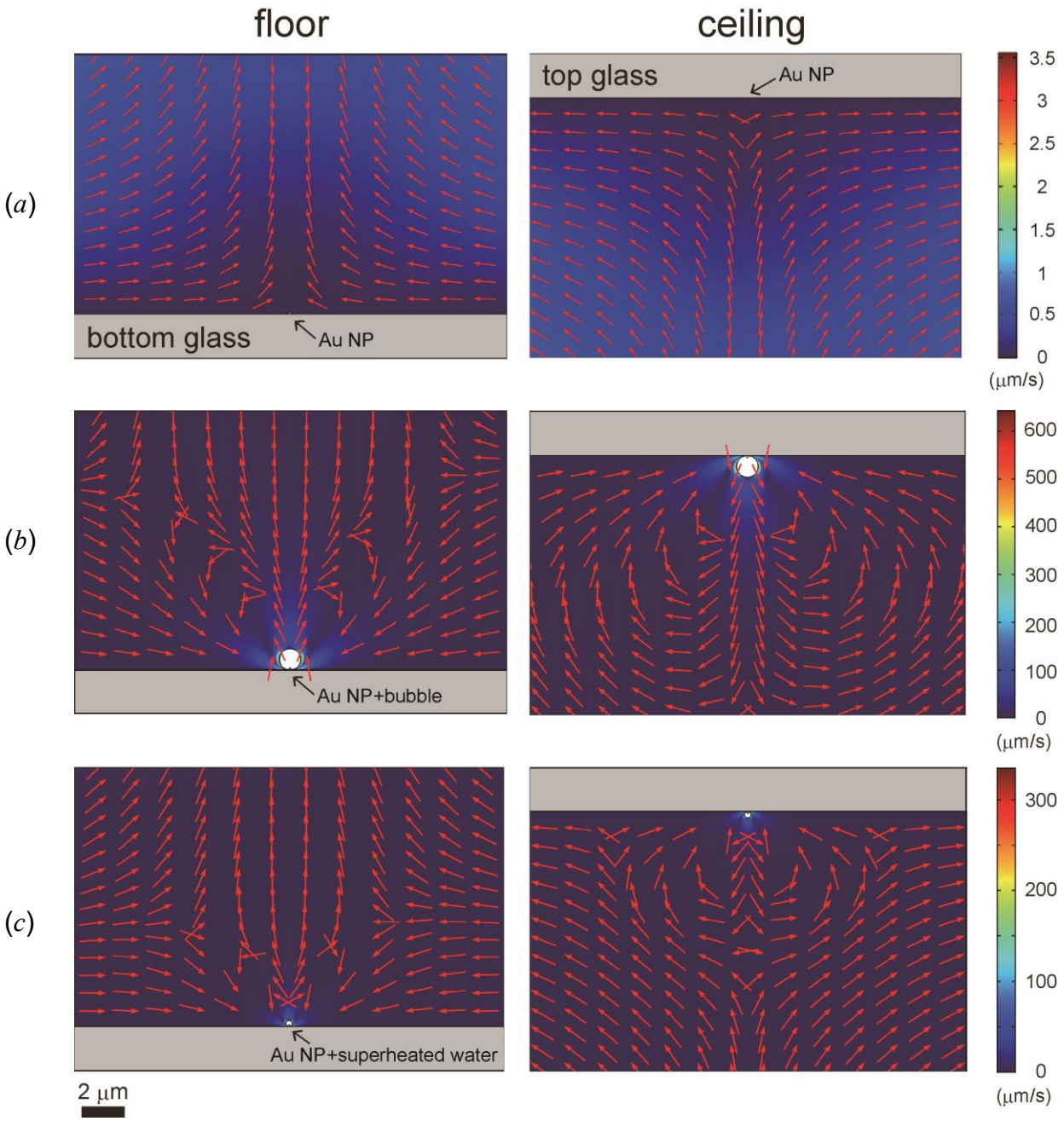

Figure 4. Simulated 2D convective velocity maps for a single water-immersed 100 nm Au NP supported on a glass substrate for floor and ceiling configurations; (*a*) solely thermal convection was accommodated (input laser intensity: 2 mW μm^{-2}), (*b*) both thermal convection in a closed chamber and Marangoni convection at the liquid water/vapor bubble (1-μm across) interface were considered (input laser intensity: 10 mW μm^{-2}), (*c*) thermal convection in the chamber space and Marangoni convection at the liquid water/superheated water (0.3-μm across) interface were considered (input laser intensity: 6 mW μm^{-2}). The calculated maximum flow velocity: 3.6 μm s^{-1} (*a*), 630 μm s^{-1} (*b*), 340 μm s^{-1} (c). The experimentally observed maximum velocity of Si-OH particles: 30 μm s^{-1} (at 6 mW μm^{-2}) and > 100 μm s^{-1} (at 14 mW μm^{-2}).

---

various input conditions (the corresponding temperature maps were given in Supporting Information, Figure S9). In *a*, solely thermal convection was accommodated. In *b*, both thermal convection in a closed chamber and Marangoni convection at the liquid water/vapor microbubble interface were considered. Experimental and computational studies on Marangoni effect associated with photothermal bubbles have been performed previously.[27-29,33-36] In *c*, thermal convection in a chamber space and Marangoni convection at the liquid water/superheated water interface were considered. We will explain the detail of this liquid water/superheated water interface later. The experimental two configurations, floor and ceiling, of Au NP were included in simulation. It turned out that water flows including their velocities for ceiling configuration exhibited a 2π rotational symmetry to that of floor configuration.

Figure 4*a* compares the calculated thermal convection flow map of floor configuration with that of ceiling. The thickness of water film was assumed as 200 μm (input laser intensity: 2 mW μm^{-2}). The flow velocities solely dependent on thermal convection were two orders of magnitude smaller than those including Marangoni effect. For instance, the calculated maximum velocity is 3.6 μm s^{-1} in Figure 4*a* whereas it is 630 μm s^{-1} in Figure 4*b*. The simulated flow map in Figure 4*a*, right confirms that the direction of thermal convection is unfavorable for trapping at ceiling. The effect of water film thickness on flow velocities was also examined (Supporting Information, Figure S10). For film thickness of 10 μm, the maximum velocity was ~10^{-3} μm s^{-1}, a value three orders of magnitude smaller than that obtained at 200 μm of thickness because of negligibly small contribution of thermal convection. The experimental maximum flow velocity of Si-OH particles undergoing trapping was 30 μm s^{-1} at the thicknesses of 10 and 200 μm (Figure 3, measured at 6 mW μm^{-2}). This confirms that the thermal convection should be too slow to account for the velocities of Si-OH particles resulting in trapping.

Contrastingly, when a bubble of 1-μm-diameter surrounding a Au NP is placed (Figure 4*b* and magnified images, Supporting Information, Figure S11 that shows the flows next to the bubble), remarkably increased flow velocities were obtained because of Marangoni convection generated at

the interface. The Marangoni convection of water along the water/vapor bubble interface is driven by surface tension gradient that is caused by the temperature gradient.[40,41] As the surface tension of water decreases with temperature, flows can be generated in the direction of cold area at the zenith of a bubble along the interface from the hot region neighboring a Au NP supported on a substrate. The simulation suggested that tangential flows pointed to the bubble and deviated away from the heating center and later redirected toward the bubble again, causing circulating flows in the areas between the substrate supporting the irradiated Au NP and the bubble (see Figure S11). The flows thus generated are favorable for trapping in both configurations. We envisage that Si-OH particles are transported to a bubble and trapped, possibly by flowing into the space between the substrate and the bubble. The experimentally observed trapping of Si-OH particles was laser intensity-dependent: the particles were attracted to a hot Au NP and a stable trapping occurred at laser intensities ≥ 0.5 mW μm^{-2}. Moreover, remarkably enhanced velocities of attracted particles simultaneously with increased number of trapped particles were observed at laser intensities ≥ 10 mW μm^{-2}, presumably because of bubble formation. The COMSOL simulation given in Figure 4*b* is consistent with the experimental observation at laser intensities ≥ 10 mW μm^{-2}.

We also observed a stable trapping at intensities between 0.5 and 8 mW μm^{-2} where we assume that a photothermal microbubble may not form based on the discontinuity observed in Figure 2. However, we cannot completely deny the potential formation of a photothermal nanobubble (< 1 μm) at ≤ 8 mW μm^{-2}. According to the observation by the Baffou group, microscopically observable microbubbles ranging from 4.6 to 64-μm-diamter occurred in aerated water at particle temperatures between 220 and 240°C (493 and 513 K) on CW laser illumination of the uniform hexagonal array of Au NPs (28 nm in diameter featuring an interparticle distance of 72 nm).[42] The temperature is much higher than the boiling temperature of water (100°C under atmospheric pressure) but lower than the spinodal decomposition temperature of water (~320°C or ~593 K). Experimentally determined microbubble formation threshold, 8 mW μm^{-2} corresponds to the particle temperature of 550 K estimated computationally (Supporting Information, Figure S4),

which is not significantly different from the value estimated by the Baffou group.[42] For heating a single Au nanotrench, the Richardson group observed the threshold temperature of bubble formation at 580±20 K, which they considered the spinodal decomposition temperature of superheated water.[43] Note that their temperature estimation relied upon indirect method.

At temperatures above 100°C, water that does not boil was considered as superheated water. For the bubble formation to occur from superheated water, a nucleation center is needed below the spinodal decomposition temperature while a nucleation center is not needed above the spinodal temperature. It has been reported that not a stable but a randomly oscillating nanobubble (oscillation period of 30 ns and frequency of ~30 MHz) occurred when a superheated water layer is formed around a Au NP at particle temperatures below the stable bubble formation threshold.[44] Although the characterization of such dynamic bubbles is extremely challenging because of the necessity of super-resolution microscopy and very fast time resolution under continuous excitation, it is most likely that photothermal nanobubbles form from superheated water at temperatures below the temperature threshold observed for microbubbles. Thus, for simplicity, we assumed a liquid water/superheated water liquid/liquid interface to approximate stable and/or fast oscillating nanobubbles that may form surrounding a heated 100-nm Au NP (we assumed 0.3-μm diameter superheated sphere supported on a glass substrate for calculation). Figure 4*c* shows the COMSOL simulation of Marangoni convection at such a liquid/liquid interface. Water flows similar to the water/microbubble interface were obtained. The flow velocities in Figure 4*c* were smaller than those in Figure 4*b*. Although not quantitative, our approximation stands for the experimental observation of trapping at laser intensities where a microbubble is not formed. Based on the simulated temperature and flow maps, we believe that Si-OH particles are attracted to the hot area around a Au NP and trapped driven by interfacial thermal Marangoni effect. Importantly, the trapping in the absence of microbubble (possibly in the presence of nanobubble) occurs in a similar manner to that in the presence of microbubble. Nevertheless, the effect of microbubble should be much greater.

Previously, the optothermal trapping of microparticles has been reported through laser heating a thin metallic or nano-island film deposited on the top of a lower substrate.[12,14] Assuming thermal convective flows inside the chamber, Flores-Flores and coworkers reported that the fluidic water was supposed to move upwards and then moves along the upper surface followed by the moves downwards at the edges and back towards the center along the lower surface.[12] The good agreement between the experimental observation and the simulated flow has prompted the following interpretation: the particles are dragged towards the beam's center by the convection currents (Stokes drag force) allowing trapping with low powers. However, as we observed, the motion of Si-OH particles directed to a hot Au NP placed at ceiling as well as floor in a closed chamber. This result cannot be explained by thermal convection that is in the opposite direction at ceiling. We also exclude thermophores from interpreting the present observation because this mechanism may not adequately describe thermophilic migration for polymers and colloids with $D_T > 0$ as we stated in the introduction.

Without heating a Au NP, no observations of particle-trapping were made. For instance, a focused illumination on the surface of a glass substrate at 20 mW μm^{-2}, which is at least 10-times greater in intensity than the typical intensity of optothermal trapping, did not allow the optical trapping of Si-OH particles. Moreover, we failed to observe the trapping event both at floor and at ceiling. In 2D optical trapping of multiple particles, the contribution of a scattering force that pushes the particles to a substrate is significant.[45] This may mean that the contribution of optical forces is not so great although optical trapping cannot be completely eliminated at much higher laser intensities. Consequently, the optical forces may not be sufficiently large because of moderate focusing using an objective of NA, 0.70 in our experiment.

Previous simulation studies demonstrated that thermos-osmosis can also induce a convective flow.[46,47] Thermo-osmotic flow arises at a solid/liquid interface as a result of tangential temperature gradient (∇T).[39] The fluid can be pushed toward the hotter or colder region depending on the nature of interaction (*ie*. the sign of χ: thermos-osmotic coefficient). Yang and coworkers performed a

simulation to investigate fluid transport driven by thermo-osmosis in microfluidic system.[46] When a hot particle was placed at a flat solid/liquid boundary, two types of flow were generated depending on the sign of S_T or D_T of moving particles. For thermophobic ($D_T > 0$) particles, a tangential flow along the wall to the hot particle moved upwards near the particle and then circulated on the particle's periphery. On the other hand, for thermophilic particles ($D_T < 0$), the flow direction was opposite: a tangential flow along the wall moving away from the hot particle was generated. At temperatures above 285 K, silica particles in water have been shown as thermophobic[25,48,49] and Si-OH particles can migrate to a hot Au NP along the wall provided that the thermos-osmosis applies in the present experiment. However, we should point out that the discussion given by Yang and coworkers is rather qualitative. It has also been suggested that the migration velocity solely dependent on thermos-osmosis can be very slow.[50] At this moment, further experiment that supports the positive role of thermos-osmosis is needed as well as simulation that convince us of its reliability.

We noted that PS particles were not stably trapped optothermally in the present study. Polystyrene particles suspended in water have been reported as thermophobic ($D_T > 0$) as Si-OH particles[51,52] and were expected to behave in a similar manner to Si-OH particles. One reason is ascribed to the spatial distribution characteristic to PS particles. As shown in Supporting Information, Figure S12, PS particles were highly concentrated at the area near the glass substrate (< 20 μm) whereas Si-OH particles were homogeneously distributed regardless of the distance from the glass surface. The high particle density near the surface can be indicative of the interaction of PS with the glass surface, impeding PS particles from migrating to the hot Au NP. The other reason might be a weak trapping stiffness of PS driven by optothermal method. Previously, Kang and coworkers observed the trapping of PS particles through heating a Au nanoisland film.[14] They used an open chamber and such a sample structure might promote a strong Marangoni flow at the air/water interface.

At laser powers below the threshold of photothermal microbubble formation, some

researchers reported the ring formation of trapped particles. For instance, Flores-Flores and coworkers observed that trapped silica microparticles formed a ring around the focused laser beam.[12] They used an amorphous silicon film for the heating medium. Their interpretation for the ring formation was based on two competing forces: Stokes drag (attraction to hot area) of thermal convection and thermophoretic forces to push out of a hot area so that tracer particles can go outside. Likewise, Shoji and coworkers observed a ring formation for the plasmon-enhanced optical trapping of PS particles using a Au nanostructured film.[53] Their interpretation was based on the competition between an attractive optical drag force and a repulsive thermophoretic force. In our experiment, no such rings were formed. The big difference is that we used a single Au NP (d = 100 nm) that is smaller than the illuminating laser beam (FWHM = 0.6 μm) for heat generation with well-defined r^{-1} spatial temperature decay profile. Contrastingly, in the above two studies, at least the area of a laser beam size (~10 μm for Flores-Flores [12] and 5 μm for Shoji[53]) was heated. Thus these much greater heating area caused by illuminating films can be responsible for the ring observation.[54] The confinement of heating area is one of the advantageous features characteristic of single particle heating.

Very recently, Winterer and coworkers reported the thermocapillary (Marangoni) convection-induced optofluidic transport of Au NPs.[13] Heating a 55% aqueous PEG solution with a near IR laser at the air/liquid interface generated a local temperature gradient and liquid motion due to thermal and thermocapillary convection. Note that they used an open chamber in which water film was exposed to air at the top surface. PEG was added to increase the viscosity, resulting in reduced thermal convection. An 80-nm Au NP suspended in a sample was dragged along the flowlines and moved away from the hot area. Interestingly, the motion of Au NPs driven by the flow near the surface was in the reverse direction to Si-OH particles in our experiment. This study demonstrated the importance of Marangoni effect in driving the flow-induced transport of nanoparticles.

Conclusion

Optothermally-inducing a fluidic motion can be a powerful way of controlling transport of macromolecules and nanoparticles at mW-range low powers. We used a single Au NP as a platform for generating liquid flows. We demonstrated that, when illuminated with a heating laser, a single Au NP acted as a trapping site for submicron Si-OH particles that moved along with liquid flows. As a mechanism of trapping, temperature-induced Marangoni effect at the liquid water/superheated water interface around the Au NP is most likely although such a driving mechanism still needs a further experimental proof. Consistent with the assumption, thermophobic (positive D_T) Si-OH particles are driven by a tangential flow to a hot area and trapped next to the Au NP. Previously, we observed that both thermoresponsive PNIPAM and non-thermoresponsive SDS or PEG were alike conveyed to a hot Au NP. The former exhibited reversible trapping, a phase-separated droplet formation, whereas the latter resulted in the coating of a Au NP. These findings highlighted an application of optothermal trapping. A single Au NP platform has an advantage of greater confinement of the heating area than that of metal films or metal nano-island films subjected to laser illumination. This highly local nature of heating enabled the absence of a ring-shaped particle assembly observed for metal film heating. Presently, we demonstrated that we remotely manipulated Si-OH particles by guiding to a hot target as a manner similar to the previously-demonstrated microbubble-induced Marangoni convection, which has a greater trapping ability but is thermally-destructive to the host material. Other studies have revealed that a Au NP can be guided by an optical gradient force to an intended position, being photothermally fixed on a substrate.[47,55] By combining this optical trapping-fixing technique with our optothermal flow generation, we can guide multiple molecules to a desired place for trapping and accumulation. This combined technique can be useful for preparing coated NPs or developing small-scale phase separation almost anywhere at the micro- and nanoscale.

■ ASSOCIATED CONTENT

Supporting Information

The Supporting Information is available free of charge on the ACS Publications website at DOI: 10.1021/acs.jpcc.

Optical setup; particle images and histogram of Au NPs used in the experiment; schematic of COMSOL simulation geometry; calculated Au NP temperature as a function of laser intensity; typical images of Si-OH particles for estimating the number of trapped particles; single particle scattering spectral peak shift as a function of laser intensity; sequence photos for particle tracking; scanning electron microscope image of a Au nanoisland film; simulated temperature maps for Figure 4; effect of water film thickness on the flow velocities; magnified images of Figure 4*b*; relative particle density as a function of distance from the substrate surface (PDF).

Movie S1: movie for Figure 1*a* (AVI)

Movie S2: movie for Figure 1*b* (AVI)

Movie S3: movie for Figure 1*c* (AVI)

Movie S4: movie for Figure 1*d* (AVI)

■ AUTHOR INFORMATION

Corresponding Author

E-mail: hashichem@tokushima-u.ac.jp

ORCID

Takayuki Uwada: 0000-0003-4272-7964

Shuichi Hashimoto: 0000-0002-8020-5537

Author Contributions

J.C. performed optical measurements. T.W. performed a numerical simulation. S.H. designed the experiment. S.H. prepared the manuscript with contributions from all authors. All authors have given approval to the final version of the manuscript.

Notes

The authors declare no competing financial interest.

■ ACKNOWLEDGMENTS

Financial support from JSPS KAKENHI (No.17K05005) is gratefully acknowledged. J.C. acknowledges the Nichia-Scholarship from the University of Tokushima and S.H. acknowledges the Elekiteru-Ozaki Foundation for the Gennai-Scholarship.

References

1. Baffou, G. *Thermoplasmonics Heating Metal Nanoparticles Using Light*; Cambridge University Press: Cambridge, UK, 2017.
2. Qin, Z.; Bischof, J. C. Thermophysical and Biological Responses of Gold Nanoparticle Laser Heating. *Chem. Soc. Rev.* **2012**, *41*, 1191–1217.
3. Abadeer, N. S.; Murphy, C. J. Recent Progress in Cancer Thermal Therapy using Gold Nanoparticles. *J. Phys. Chem. C* **2016**, *120*, 4691–4718.
4. Gaiduk, A.; Ruijgrok, P. V.; Yorulmaz, M.; Orrit, M. Detection Limits in Photothermal Microscopy. *Chem. Sci*., **2010**, *1*, 343–350.
5. Bora, T.; Zoepfl, D.; Dutta, J. Importance of Plasmonic Heating on Visible Light Driven Photocatalysis of Gold Nanoparticle Decorated Zinc Oxide Nanorods. *Sci. Rep*., **2016**, *6*, 26913.
6. Xiong, Y.; Long,R.; Liu, D.; Zhong, X.; Wang, C.; Lib, Z-Y.; Xie, Y. Solar Energy Conversion with Tunable Plasmonic Nanostructures for Thermoelectric Devices. *Nanoscale*, **2012**, *4*, 4416–4420.
7. Keblinski, P.; Cahill, D. G.; Bodapati, A.; Sullivan, C. R.; Taton, T. A. Limits of Localized Heating by Electromagnetically Excited Nanoparticles. *J. Appl. Phys.*, **2006**, *100*, 054305.
8. Lin, L.; Hill, E. H.; Peng, X.; Zheng, Y. Optothermal Manipulations of Colloidal Particles and Living Cells. *Acc. Chem. Res*. **2018**, *51*, 1465−1474.
9. Neuman, K. C. Steven M. Block, S. M. Optical Trapping. *Rev. Sci. Instrum*., **2004**, *75*, 2787−2809.
10. Hansen, P. M.; Bhatia, V. K.; Harrit, N.; Oddershede, L. Expanding the Optical Trapping Range of Gold Nanoparticles. *Nano Lett*., **2005**, *5*, 1937–1942.
11. Lehmuskero, A.; Johansson, P.; Rubinsztein-Dunlop, H.; Tong, L.; Käll, M. Laser Trapping of Colloidal Metal Nanoparticles. *ACS Nano* **2015**, *9*, 3453−3469.
12. Flores-Flores, E.; Torres-Hurtado, S. A.; Páez, R.; Ruiz, U.; Beltrán-Pérez, G.; Neale, S. L.; Ramirez-San-Juan, J. C.; Ramos-García, R. Trapping and Manipulation of Microparticles using

Laser-induced Convection Currents and Photophoresis. *Biomed. Opt. Express*, **2015**, *6*, 4079–4087.

13. Winterer, F.; Maier, C. M.; Pernpeintner, C.; Lohmüller, T.; Optofluidic Transport and Manipulation of Plasmonic Nanoparticles by Thermocapillary Convection. *Soft Matter*, **2018**, *14*, 628–634.
14. Kang, Z.; Chen, J.; Wu, S.-Y. Chen, K.; Kong, S.-K. Yong, K.-T. Ho, H.-P. Trapping and Assembling of Particles and Live Cells on Large-scale Random Gold Nano-island Substrates. *Sci. Rep*. **2015**, *5*, 9978.
15. Enders, M.; Mukai, S.; Uwada, T.; Hashimoto, S. Plasmonic Nanofabrication through Optical Heating. *J. Phys. Chem. C*, **2016**, *120*, 6723–6732.
16. Aibara, I.; Mukai, S.; Hashimoto, S. Plasmonic-Heating-Induced Nanoscale Phase Separation of Free Poly(*N*-isopropylacrylamide) Molecules. *J. Phys. Chem. C*, **2016**, *120*, 17745–17752.
17. Aibara, I.; Chikazawa, J..; Uwada, T.; Hashimoto, S. Localized Phase Separation of Thermoresponsive Polymers Induced by Plasmonic Heating. *J. Phys. Chem. C*, **2017**, *121*, 22496–22507.
18. Braun, D.; Libchaber, A. Trapping of DNA by Thermophoretic Depletion and Convection. *Phys. Rev. Lett*. **2002**, *89*, 188103.
19. Duhr, S.; Braun, D. Thermophoretic Depletion Follows Boltzmann Distribution. *Phys. Rev. Lett.* **2006**, *96*, 168301.
20. Würger, A. Transport in Charged Colloids Driven by Thermoelectricity. *Phys. Rev. Lett*. **2008**, *101*, 108302.
21. Reichl, M.; Herzog, M.; Götz, A.; Braun, D. Why Charged Molecules Move Across a Temperature Gradient: The Role of Electric Fields. *Phys. Rev. Lett*. **2014**, *112*, 198101.
22. Duhr, S.; Braun, D. Why Molecules Move along a Temperature Gradient. *Proc. Natl Acad. Sci. USA*, **2006**, *103*. 19678–19682.
23. Piazza, R. Thermophoresis: Moving Particles with Thermal Gradients. *Soft Matter*, **2008**, *4*,

1740–1744.

24. Chan, J.; Popov, J. J.; Kolisnek-Kehl, S.; Leaist, D. G. Soret Coefficients for Aqueous Polyethylene Glycol Solutions and Some Tests of the Segmental Model of Polymer Thermal Diffusion. *J. Solution Chem*., **2003**, *32*, 197−214.
25. Piazza, R.; Pardola, A. Thermophoresis in Colloidal Suspensions. *J. Phys.: Condens. Matter* **2008**, *20*, 153102.
26. Kita, R.; Wiegand, S. Soret Coefficient of Poly(*N*-isopropylacrylamide)/Water in the Vicinity of Coil-Globule Transition Temperature. *Macromolecules* **2005,** *38,* 4554-4556.
27. Uwada, T.; Fujii, S.; Sugiyama, T.; Usman, A.; Miura, A.; Masuhara, H.; Kanaizuka, K.; Haga, M. Glycine Crystallization in Solution by CW Laser-Induced Microbubble on Gold Thin Film Surface. *ACS Appl. Mater. Interfaces* **2012**, *4*, 1158−1163.
28. Zheng, Y.; Liu, H.; Wang, Y.; Zhu, C.; Wang, S.; Cao, J.; Zhu, S. Accumulating Microparticles and Direct-writing Micropatterns using a Continuous-wave Laser-induced Vapor Bubble. *Lab Chip*, **2011**, *11*, 3816–3820.
29. Setoura, K.; Ito, S.; Miyasaka, H. Stationary Bubble Formation and Marangoni Convection induced by CW laser Heating of a Single Gold Nanoparticle. *Nanoscale*, **2017**, *9*, 719–730.
30. Valgaftik, N. B.; Volkov, B. N.; Voljak, L. D. International Tables of Surface Tension of Water. *J. Phys. Chem. Ref. Data*, **1983**, 12, 817–820.
31. D. R. Lide Ed., *CRC Handbook of Chemistry and Physics*, *80th Ed*.; CRC Press: Boca Raton, 1999.
32. Hartland, G. V. Optical Studies of Dynamics in Noble Metal Nanostructures. *Chem. Rev*. **2011**, *111*, 3858−3887.
33. Setoura, K.; Werner, D; Hashimoto, S Optical Scattering Spectral Thermometry and Refractometry of a Single Gold Nanoparticle under CW Laser Excitation. *J. Phys. Chem. C*, **2012**, *116*, 15458−15466.
34. Namura, K.; Nakajima, K.; Suzuki, M. Quasi-Stokeslet Induced by Thermoplasmonic

Marangoni Effect around a Water Vapor Microbubble. *Sci. Rep*. **2017**, *7*, 45776.

35. Lin, L.; Peng, X.; Mao, Z.; Li, W.; Yogeesh, M. N.; Rajeeva, B. B.; Perillo, E. P.; Dunn, A. K.; Akinwande, D.; Zheng, Y. Bubble-Pen Lithography. *Nano Lett*. **2016**, *16*, 701−708.
36. Xie, Y.; Zhao, C. An Optothermally Generated Surface Bubble and its Applications. *Nanoscale*, **2017**, *9*, 6622–6631.
37. Donner, J. S.; Baffou, G.; McCloskey, D.; Quidant, R. Plasmon-Assisted Optofluidics. *ACS Nano* **2011**, *5*, 5457−5462.
38. Maeda, Y. T. Buguin, A.; Libchaber, A. Thermal Separation: Interplay between the Soret Effect and Entropic Force Gradient. *Phys. Rev. Lett*., **2011**, *107*, 038301.
39. Bregulla, A. P. Würger, A.; Günther, K.; Mertig, M.; Cichos, F. Thermo-Osmotic Flow in Thin Films. *Phys. Rev. Lett*., **2016**, *116*, 188303.
40. Manjare, M.; Yang, F.; Qiao, R.; Zhao, Y. Marangoni Flow Induced Collective Motion of Catalytic Micromotors. *J. Phys. Chem. C* **2015**, *119*, 28361−28367.
41. Yang, X.; Baczyzmalski, D.; Cierpka, C.; Mutschke, G.; Eckert, K. Marangoni Convection at Electrogenerated Hydrogen Bubbles. *Phys. Chem. Chem. Phys.,* **2018**, *20*, 11542−11548.
42. Baffou, G.; Polleux, J.; Rigneault, H.; Monneret, S. Super-Heating and Micro-Bubble Generation around Plasmonic Nanoparticles under cw Illumination. *J. Phys. Chem. C* **2014**, *118*, 4890−4898.
43. Baral, S.; Green, A. J.; Livshits, M. Y.; Govorov, A. O.; Richardson, H. H. Comparison of Vapor Formation of Water at the Solid/Water Interface to Colloidal Solutions Using Optically Excited Gold Nanostructures. *ACS Nano* **2014**, *8*, 1439–1448.
44. Hou, L.; Yorulmaz, M.; Verhart, N. R.; Orrit, M. Explosive Formation and Dynamics of Vapor Nanobubbles around a Continuously Heated Gold Nanosphere. *New. J. Phys*. **2015**, *17*, 013050.
45. Kudo, T.; Wang, S.-F.; Yuyama, K.; Masuhara, H. Optical Trapping-Formed Colloidal Assembly with Horns Extended to the Outside of a Focus through Light Propagation. *Nano Lett*. **2016**, *16*, 3058−3062.

46. Yang, M.; Liu, R.; Ye, F.; Chen, K. Mesoscale Simulation of Phoretically Osmotic Boundary Conditions. *Soft Matter*, **2017**, *13*, 647−657.
47. Gargiulo, J.; Brick, T.; Violi, I. L.; Herrera, F. C.; Shibanuma, T.; Albella, P.; Requejo, F. G.; Cortés, E.; Maier, S. A.; Stefani, F. D. Understanding and Reducing Photothermal Forces for the Fabrication of Au Nanoparticle Dimers by Optical Printing. *Nano Lett*. **2017**, *17*, 5747−5755.
48. Shiundu, P. M.; Williams, P. S.; Giddings, J. C. Magnitude and Direction of Thermal Diffusion of Colloidal Particles Measured by Thermal Field-flow Fractionation. *J. Colloid Interface Sci*., **2003**, *266*, 366−376.
49. Regazzetti, A.; Hoyos, M.; Michel Martin, M. Experimental Evidence of Thermophoresis of Non-Brownian Particles in Pure Liquids and Estimation of Their Thermophoretic Mobility. *J. Phys. Chem. B*, **2004**, *108*, 15285–15292.
50. Peng, X.; Lin, L.; Hill, E. H.; Kunal, P.; Humphrey, S. M.; Zheng, Y. Optothermophoretic Manipulation of Colloidal Particles in Nonionic Liquids. *J. Phys. Chem. C* **2018**, *122*, 24226−24234.
51. Helden, L; Eichhorn, R.; Bechinger, C. Direct Measurement of Thermophoretic Forces. *Soft Matter*, **2015**, *11*, 2379–2386.
52. Tsuji, T.; Kozai, K.; Ishino, H.; Kawano, S. Direct Observations of Thermophoresis in Microfluidic Systems. *Micro Nano Lett*., **2017**, *12*, 520–525.
53. Shoji, T.; Shibata, M.; Kitamura, N.; Nagasawa, F.; Takase, M.; Murakoshi; K.; Nobuhiro, A.; Mizumoto, Y.; Ishihara, H.; Tsuboi, Y. Reversible Photoinduced Formation and Manipulation of a Two-Dimensional Closely Packed Assembly of Polystyrene Nanospheres on a Metallic Nanostructure. *J. Phys. Chem. C* **2013**, *117*, 2500−2506.
54. Odagiri, K.; Seki, K.; Kudo, K. Ring Formation by Competition between Entropic Effect and Thermophoresis. *Soft Matter*, **2012**, *8*, 6775–6781.
55. Urban, A. S.; Lutich, A. A.; Stefani, F. D.; Feldmann, J. Laser Printing Single Gold Nanoparticles. *Nano Lett*. **2010**, *10*, 4794–4798.

TOC Graphic (8.25 cm×4.45 cm)